Biogeosciences, 11, 7179–7192, 2014
www.biogeosciences.net/11/7179/2014/
doi:10.5194/bg-11-7179-2014

Biogeosciences Open Access

Inorganic carbon fluxes across the vadose zone of planted and unplanted soil mesocosms

E. M. Thaysen[1], D. Jacques[2], S. Jessen[3], C. E. Andersen[4], E. Laloy[2], P. Ambus[3], D. Postma[5], and I. Jakobsen[6]

[1]Instituto de Diagnóstico Ambiental y Estudios del Agua (IDAEA), CSIC, Jordi Girona 18, 08034 Barcelona, Catalonia, Spain
[2]Institute for Environment, Health, and Safety, Belgian Nuclear Research Centre (SCK CEN), 2400, Mol, Belgium
[3]Department of Geosciences and Natural Resource Management, Copenhagen University, 1350, Copenhagen, Denmark
[4]Centre for Nuclear Technologies, Technical University of Denmark, 4000 Roskilde, Denmark
[5]Department of Geochemistry, Geological Survey of Denmark and Greenland, 1350, Copenhagen, Denmark
[6]Department of Chemical and Biochemical Engineering, Centre for Ecosystems and Environmental Sustainability, Technical University of Denmark, 2800, Kongens Lyngby, Denmark

Correspondence to: E. M. Thaysen (eikethaysen@idaea.csic.es)

Received: 1 October 2013 – Published in Biogeosciences Discuss.: 17 March 2014
Revised: 1 November 2014 – Accepted: 12 November 2014 – Published: 17 December 2014

Abstract. The efflux of carbon dioxide (CO_2) from soils influences atmospheric CO_2 concentrations and thereby climate change. The partitioning of inorganic carbon (C) fluxes in the vadose zone between emission to the atmosphere and to the groundwater was investigated to reveal controlling underlying mechanisms. Carbon dioxide partial pressure in the soil gas (pCO_2), alkalinity, soil moisture and temperature were measured over depth and time in unplanted and planted (barley) mesocosms. The dissolved inorganic carbon (DIC) percolation flux was calculated from the pCO_2, alkalinity and the water flux at the mesocosm bottom. Carbon dioxide exchange between the soil surface and the atmosphere was measured at regular intervals. The soil diffusivity was determined from soil radon-222 (^{222}Rn) emanation rates and soil air Rn concentration profiles and was used in conjunction with measured pCO_2 gradients to calculate the soil CO_2 production. Carbon dioxide fluxes were modeled using the HP1 module of the Hydrus 1-D software.

The average CO_2 effluxes to the atmosphere from unplanted and planted mesocosm ecosystems during 78 days of experiment were 0.1 ± 0.07 and 4.9 ± 0.07 µmol C m^{-2} s^{-1}, respectively, and grossly exceeded the corresponding DIC percolation fluxes of 0.01 ± 0.004 and 0.06 ± 0.03 µmol C m^{-2} s^{-1}. Plant biomass was high in the mesocosms as compared to a standard field situation. Post-harvest soil respiration (R_s) was only 10 % of the R_s during plant growth, while the post-harvest DIC percolation flux was more than one-third of the flux during growth. The R_s was controlled by production and diffusivity of CO_2 in the soil. The DIC percolation flux was largely controlled by the pCO_2 and the drainage flux due to low solution pH. Modeling suggested that increasing soil alkalinity during plant growth was due to nutrient buffering during root nitrate uptake.

1 Introduction

The global flux of carbon dioxide (CO_2) from the soil to the atmosphere amounts to 59–76.5 Gt carbon (C) yr^{-1} and is one of the largest fluxes in the global C budget (Raich and Potter, 1995; Houghton, 2007). Agriculture strongly enhances this flux, accounting for 10–12 % of global anthropogenic emissions (Robertson et al., 2000; Barker et al., 2007; Vermeulen et al., 2012). The flux of CO_2 from the soil to the groundwater as dissolved inorganic carbon (DIC) is estimated at 0.2 Gt C yr^{-1} and is hence much less than the upward flux of CO_2 (Kessler and Harvey, 2001). Agriculture enhances the DIC percolation flux by up to 4 times compared to undisturbed systems (Barnes and Raymond, 2009). Although numerous measurements have been made of either gas or aqueous phase CO_2 emission from cropland to

the atmosphere and groundwater, respectively, few studies have investigated the total CO_2 emission with regard to its controls. In the light of the climate change induced by the present atmospheric concentration of CO_2 of 400 ppm and its increment rate of $\sim 2\,\mathrm{ppm\,yr^{-1}}$ (IPCC, 2007; Lal, 2011), the magnitudes and underlying mechanisms of the soil CO_2 effluxes to the atmosphere and groundwater from agricultural systems are of crucial importance for prediction of the climate forcing. The residence time of DIC in groundwater is at least as long as the residence time of groundwater itself, which may be in the order of hundreds to thousands of years (Kessler and Harvey, 2001). The atmospheric residence time of CO_2 may be as low as 5 years (Solomon et al., 2007; Archer and Brovkin, 2008) implying that even small changes in the C emission balance can have important effects on the atmospheric CO_2 concentration (Schimel, 1995). The present study explores the total CO_2 emission for a cropland mesocosm system and investigates the underlying mechanisms.

The soil partial pressure of CO_2 (pCO_2) and the soil CO_2 efflux to the atmosphere, also referred to as the soil respiration (R_s), are a function of the combined CO_2 production from microorganisms and roots, the soil gas diffusivity and a limited contribution from mineral reactions via the carbonate system (Kuzyakov, 2006; Trumbore, 2006). Soil temperature and moisture are the main abiotic factors controlling the biological production of CO_2 (Schlesinger, 1973; Maier et al., 2011). Further factors such as the overall soil nutrient content, soil mineralogy, land use history and plant phenology also play an important role for the magnitude of the soil CO_2 production (Lohila et al., 2003; Trumbore, 2006).

Diffusion of CO_2 in air is about 10^4 times faster than in water (Suarez and Šimůnek, 1993). Rain increases the R_s due to a stimulation of microbial respiration and/or due to displacement of CO_2-rich soil air by advection (Huxman et al., 2004, Lee et al., 2002). However, frequent and heavy rains eventually result in a high soil water content that lowers the soil gas diffusivity, leading to accumulation of CO_2 in air-filled pores (i.e., higher pCO_2) and a reduced R_s (Jassal et al., 2005; Zhang et al., 2010).

Dissolved inorganic carbon is the sum of C in carbonic acid, $H_2CO_3^*$ (where $H_2CO_3^* = CO_{2(aq)} + H_2CO_3$), bicarbonate, HCO_3^-, and carbonate, CO_3^{2-}. The concentration of DIC, [DIC], is closely linked to the pCO_2 via Henry's law. In addition, the [DIC] depends on soil solution chemistry because of the pH-dependent solubility of inorganic C species, and is as such largely influenced by processes that increase soil alkalinity, e.g., the weathering of carbonate and silicate minerals (Appelo and Postma, 2005; Walmsley et al., 2011). The DIC percolation flux to the groundwater can be described by multiplying the [DIC] by the recharge flux (Appelo and Postma, 2005; Thaysen et al., 2014a).

Here, we measured upward and downward CO_2 transport in both gas and aqueous phases in unplanted and planted mesocosms to quantify the total CO_2 emission from ecosystems. The mesocosms, established to simulate the top 0–80 cm soil profile of a barley cropland, were incubated under controlled environmental conditions, allowing a model-based investigation (HP1 module, Hydrus 1-D) of the biogeochemical controls on CO_2 production and transport in the soil profile prior to seeding, during growth and after harvest. Mesocosms have been shown to provide useful environments for conducting process-related research in unsaturated soil (Hendry et al., 2001; Thaysen et al., 2014a). Reactive transport modeling may further increase the understanding of the coupled physical, chemical, and biological processes influencing CO_2 transport within soils (Steefel et al., 2005). HP1 allows for the complex biogeochemical modeling of CO_2 transport in the vadose zone by providing options for simulation of soil water content, root growth, root water and solute uptake, as well as for gas diffusion and geochemical reactions of all possible chemical species, the latter being a novelty amongst vadose zone models.

2 Methodology

2.1 Setup of mesocosms

Emissions of CO_2 and DIC from unplanted and planted soil profiles may be directly compared in equally structured and textured soil maintained under controlled environmental conditions. In this study, seven mesocosms were constructed and incubated in a climate chamber. A detailed description of the experimental set-up and filling of mesocosms is given in Thaysen et al. (2014a). Soil was collected from the A and C horizon of an experimental field site located in an agricultural area (Voulund, Denmark, 56°2′35.7 N, 9°8′101.1 E) characterized as a coarse–sandy alluvial sediment (Podzol). The soil was sieved (6 mm) and packed into plexiglas cylinders (length: 85 cm, diameter: 19 cm) (Fig. 1a). The A and C horizons were located at 0–30 and 30–78.5 cm depth, respectively. The bottom plate of the mesocosms at 82–85 cm had an embedded suction disc (thickness of 10 mm) and the hydraulic connection between the C horizon and the suction disc was optimized by means of a thin layer of quartz flour ($\sim$ 81.5–82 cm) and a layer of quartz flour mixed with C horizon ($\sim$ 78.5-81.5 cm).

The mesocosms were subjected to different treatments (Table 1). Two mesocosms remained unplanted (referred to as the unplanted treatment). These mesocosms were shown to exhibit low variability and high reproducibility (Thaysen et al., 2014a). To investigate the additional variability introduced by the presence of plants, barley (*Hordeum vulgare L.* cv Anakin) was sown into three mesocosms. In these mesocosms CO_2 fluxes were investigated during growth (days 14 to 58 after sowing) and after harvest (days 58–117) (referred to as the barley growth treatment #1 and the post-harvest treatment, respectively). The agreement between mesocosms remained good (Figs. 3, S1 in the Supplement), also allowing

Table 1. Overview over mesocosm experiments. The post-harvest experiment was the successive of the barley growth experiment #1.

Treatment	Duration of experiment (days)	Fertilization
Barley growth #1	58	Addition to soil prior to experiments
Barley growth #2	78	Nutrient irrigation
Post-harvest (post growth #1)	60	Addition to soil prior to experiments
Unplanted	78	Nutrient irrigation

for a reduction to a sample size of two for planted mesocosms. In further two mesocosms the growth period of barley was extended to 100 days with monitoring up to 78 days after sowing (barley growth treatment #2). In each planted mesocosm, 15 barley seeds were sown at 3 cm depth, and upon germination the seedlings were thinned to eight per mesocosm, corresponding to 280 plants m^{-2}.

Prior to packing of the mesocosms for the barley growth treatment #1, basal nutrients were mixed into the upper 9 cm of the A horizon in the following amounts (mg kg^{-1} soil): NH_4NO_3, 30; K_2SO_4, 75; $CaCl_2$,75; $MgSO_4 \times 7H_2O$, 45; $MnSO_4 \times H_2O$, 10.5; $ZnSO_4 \times 7H_2O$, 5.4; $CuSO_4 \times 5H_2O$, 2.1; Na_2MoO_4 $2H_2O$, 0.2; $CoSO_4 \times 7H_2O$, 0.4. Mesocosms in the barley growth #1 and post-harvest treatment were irrigated with milli-Q water at 1–2 days intervals throughout the experiment. Mesocosms in the barley growth treatment #2 were irrigated in the same manner before day 56 and thereafter daily, however, irrigation was with milli-Q water prior to germination of barley and subsequently with a 50 % strength Hoagland nutrient solution (Hoagland and Amon, 1950). The different mode of fertilizer application for the second barley growth treatment was implemented in order to avoid nutrient depletion of the soil during the longer experimental runtime. Unplanted mesocosms were initially irrigated using similar irrigation amounts as for planted mesocosms to compare the magnitude of soil respiration in unplanted and planted soil. Irrigation amounts were decreased after 24 days due to observed water logging at the mesocosm bottoms, but topsoil volumetric water content (VWC) was maintained at approximately the same level as in barley mesocosms (Fig. S1). Average irrigation amounts for the barley growth #1, the barley growth #2, the post-harvest and the unplanted treatments were 5.3, 13.5, 4.6 and 4.4 mm d^{-1}, respectively. Irrigation amounts exceeded those in the typical field situation because soil temperatures and plant biomass in mesocosms were elevated, leading to higher evapotranspiration (see Sect. 4.1). Maintenance of mesocosms was as in Thaysen et al. (2014a).

Figure 1. Mesocosm system with barley plants and sampling ports for gas and water sample collection, soil moisture and temperature measurement **(a)** and setup for CO_2 exchange measurements **(b)**. During experiments, mesocosms were shaded from light with dark plastic bags.

2.2 Sampling and calculations

Due to the limited amount of replicates in this study, we report data ranges instead of averages for all our core measurements. Ranges represent either the smallest and highest measured value for the barley growth #1 and the post-harvest treatment or both values for the barley growth #2 and the unplanted treatment.

2.2.1 Inorganic C speciation calculations and DIC percolation

Soil water alkalinity ($\sim$ sum of $[HCO_3^-]$ and $2 \times [CO_3^{2-}]$), soil pCO_2, soil temperature and moisture content were determined as function of depth and time, as described in Thaysen et al. (2014a). The speciation of inorganic C was calculated from the pCO_2, alkalinity and soil temperature using PHREEQC (Parkhurst and Appelo, 2013). The weekly DIC percolation flux in each mesocosm was estimated from the calculated [DIC] at the lowest sampling depth and the measured drainage flux. When low pCO_2 was measured at the

mesocosm bottoms due to high water content (see Thaysen et al. 2014a), the upper next sampler was used to obtain the pCO_2 value.

2.2.2 CO_2 exchange

The exchange of CO_2 between the soil surface of the mesocosms and the atmosphere was measured using the static closed chamber technique (Ambus et al., 2007). A transparent cylindrical chamber ($V = 22.6$ L) was carefully mounted gastight (Terostat sealant) on the mesocosm tops. Before deployment, the chamber was filled with air of ambient CO_2 concentration. During measurement, the pCO_2 in the chamber space was closed-loop analyzed continuously with an environmental gas monitor (EGM-2, PP-Systems, Amesbury, MA, USA) (Fig. 1b), and the CO_2 flux was estimated from the concentration change, volume and measurement time. Carbon dioxide exchange in barley mesocosms was measured under light and in the dark to quantify net ecosystem exchange (NEE) and ecosystem respiration (ER, R_s+ canopy respiration), respectively. The barley plant canopy occupied an area that was approx. 4 times the surface area of the mesocosm, which implied careful insertion of shoots into the measurement chamber (Fig. 1). For unplanted mesocosms, only R_s was measured.

2.2.3 Radon profiles

Sedimentary produced radon-222 (^{222}Rn) was measured at different VWCs for unplanted mesocosms and mesocosms of the barley growth #1 treatment, in order to determine the soil diffusivity. Evacuated ZnS(Ag)-scintillation cells ($V = 200$ mL) equipped with a manometer were attached to the mesocosm gas sampling ports. The scintillation cells were removed when their internal pressure had increased to 1013 hPa. Samples were analyzed on a scintillation counter (EDA-200, CAN). The background activity of Rn-222 inside the climate chamber was measured with an Alphaguard PQ-2000 (Alphaguard, Genitron, DE) and was about 100 Bq m^{-3}. Radon emanation rates of each soil horizon were determined in the laboratory from five replicate soil aliquots of 200 g through incubation in a closed container for 2 months and subsequent scintillation counting of an air sample from the container. Experimentally determined Rn profiles were modeled with the RnMod3d software (Andersen, 2001) using measured VWCs and Rn emanation rates and assuming homogeneity within each soil horizon. Resulting bulk diffusivities were then used in the modeling of the CO_2 (Sect. 2.3) and to estimate the soil CO_2 production rate, R_{CO_2}, (μmol m^{-2} s^{-1}) from Fick's first law of diffusion (e.g., Fierer et al., 2005):

$$R_{CO_2} = D_{soil} \cdot (C_T - C_B)/z, \quad (1)$$

where D_{soil} (m^2 s^{-1}) is the bulk CO_2 diffusion coefficient in the A horizon soil, C_T is the concentration of CO_2 at the mesocosm surface (μmol m^{-3}), C_B is the concentration of CO_2 at the sampling depth of peak pCO_2 (μmol m^{-3}), and z is the depth interval (m). The variable D_{soil} was determined by dividing the CO_2 diffusion coefficient in air with the ratio between the Rn diffusion coefficient in air and the Rn bulk diffusion coefficient for the A horizon. Equation (1) assumes isobaric conditions, no downward flux of CO_2 beyond C_B, and CO_2 transport by gaseous diffusion only. It also neglects the effect of spatial differences in VWC.

2.2.4 Evapotranspiration

Weekly evapotranspiration was estimated from the difference between calculated and measured mesocosm weights. The calculated weight of a given mesocosm was obtained by subtracting the water removal due to effluent and sampling, from the sum of the mesocosm weight and the volume of irrigation water.

2.3 Modeling of CO_2 fluxes

In order to determine the controls on gaseous and dissolved CO_2 fluxes, results from barley growth experiments were modeled using the HP1 module of the Hydrus software (Šimůnek et al., 2006; Jacques et al., 2008). Due to the similarity between mesocosms (Figs. 3, S1), only simulation results of one mesocosm from the second barley growth experiment are presented herein. Besides the coupling between variably-saturated water flow, multicomponent transport, heat transport and biogeochemistry, particular features of the conceptual model are (i) CO_2 production accounting for respiration of both soil organisms and plant roots based on the SOILCO$_2$ model (Šimůnek and Suarez, 1993; Suarez and Šimůnek, 1993), linking explicitly soil respiration to root growth, (ii) cation exchange reactions and geochemical buffering by minerals, and (iii) root growth and root solute uptake.

2.3.1 Model setup

The mesocosm model contained three materials. The first two materials represented the A- and C horizons, respectively. The suction plate at the bottom of the mesocosm, the quartz flour layer and the layer of quartz flour mixed with the C horizon were lumped in the third material at 80–83 cm depth. The model domain was discretized in 157 nodes with the highest node densities at the mesocosm top and at the interfaces of the soil materials. Water flow was described by the Richards equation (Richards, 1931) and the constitutive relations of the van Genuchten–Mualem model without hysteresis (Mualem, 1978; van Genuchten, 1980). Upper boundary conditions for the water flow accounted for temporally variable irrigation rates and potential evapotranspiration, which was modeled using weekly estimates (Sect. 2.2.4). At the domain bottom, a variable pressure head boundary condition was used to account for the applied suction range of −0.1

to −0.75 bar relative to atmospheric pressure (Thaysen et al., 2014a). The root depth was fixed at 30 cm throughout the experiment, corresponding to a measured root depth of 30 cm on simulation day 0 (day 15 after sowing) and allocation of ∼ 90 % of the root mass in the A horizon at the end of the experiment (as measured in a similar experiment; Thaysen et al. 2014b). A normalized exponential root distribution function was employed to describe the vertical root distribution within the A horizon (Hoffmann and van Genuchten, 1983). Root water uptake was modeled using the root distribution and the S-shaped water uptake model without solute stress and default parameterization (van Genuchten, 1987). Water retention parameters were obtained from inverse modeling of the water flow in an unplanted mesocosm (data not shown) using Hydrus 1-D (Šimůnek et al., 2013) and a global stochastic optimization algorithm (Vrugt et al., 2009).

Solute transport was modeled with the advection-dispersion equation. Carbon dioxide transport processes included in HP1 are diffusion in the gas phase and advective-hydrodynamic dispersion in the aqueous phase. Carbon dioxide diffusion in the water and gas phase, respectively, was modeled by scaling the CO_2 diffusion coefficient in water and air with the Millington and Quirk tortuosity (Millington and Quirk, 1961). The boundary layer height was set at 0.02 m. Equilibrium CO_2 distribution between the gas and the water phase is described in HP1 by Henry's law. More details are available in Šimůnek et al. (2006) and Jacques et al. (2008).

Heat transport was also described with an advection-dispersion equation using thermal conductivity data for sand (Chung and Horton, 1987). Soil temperatures of 22 and 18 °C were chosen for the upper and lower boundary conditions, respectively, corresponding to the measured temperature decline from the top to the bottom of the mesocosm (Fig. S1). Day and night cycles were modeled with temperature amplitudes of 5 °C.

2.3.2 CO_2 production and root growth

Soil CO_2 production was modeled through implementation of equations and parameters from the SOILCO$_2$ model (Šimůnek and Suarez, 1993; Suarez and Šimůnek, 1993), making a few modifications. The total CO_2 production rate, S(mol m^{-2} s^{-1}), is considered as the sum of the production by the soil microorganisms, γ_s (mol m^{-2} s^{-1} g_{DWroot}^{-1} (g_{DWroot}^{-1}; grams dry weight root biomass)), and the production by plant roots, γ_p (mol m^{-2} s^{-1} g_{DWroot}^{-1}), according to

$$S = (\gamma_s + \gamma_p)\mathrm{RMI}, \quad (2)$$

where the subscripts s and p refer to soil microorganisms and plant roots, respectively, and RMI is the root mass index in the system (g DW). Both γ_p and γ_s were linked to the root distribution, since microbial respiration is primed by root mass (Kuzyakov, 2002; Zhu and Cheng, 2011). It is assumed that individual CO_2 producing processes are additive and that it is possible to superpose individual mechanisms that reduce production from an optimal value. The production rates for microbial and root respiration at any given point in time and space are described by Eqs. 3–5

$$\gamma_s = \gamma_{s0} \prod_i f_{si}, \quad (3)$$

$$\gamma_p = \gamma_{p0} \prod_i f_{pi}, \quad (4)$$

$$\prod_i f_i = f(h)\, f(T)\, f_{CO_2}(c_a)\, f(h_\emptyset)\, f(z), \quad (5)$$

where γ_{s0} and γ_{p0} are the optimum respiration rates for microorganisms and roots (mol m^{-2} s^{-1} g_{DWroot}^{-1}), respectively, and the term Πf_i multiplies all reduction coefficients. The coefficient $f(h)$ is the reduction coefficient as a function of pressure head (unitless), $f(T)$ is the reduction coefficient as a function of temperature (unitless) and $f_{CO_2}(c_a)$ is the reduction coefficient as a function of CO_2 concentration (reduced oxygen availability) (unitless). These coefficients are assumed to be equal for γ_{s0} and γ_{p0}. The coefficient $f(h_\emptyset)$ is the reduction coefficient as a function of osmotic head (unitless) which is set to 1 for γ_{s0} (no reduction). Expressions for all reduction coefficients except for the reduction coefficient as a function of depth in the soil profile (m^{-1}), $f(z)$, are identical to those in SOILCO$_2$, more details are available in Šimůnek and Suarez (1993). The coefficient $f(z)$ is described differently for γ_{s0} and γ_{p0}, as defined below. All reduction terms have values between 0 and 1, except the $f(T)$ which is higher than 1 above 20 °C and smaller than 1 below 20 °C.

Increasing CO_2 production due to the evolving root mass, RMI, is described by a linear biomass increase with time:

$$\mathrm{RMI} = R_{\mathrm{init}} + (\mathrm{time} \cdot r), \quad (6)$$

where R_{init} is the initial root mass at simulation time zero (g DW), and r is the root growth rate (g s^{-1}).

The depth reduction factor for root respiration, $f_p(z)$, is directly linked to the modeled vertical root distribution. For the microbial respiration, $f_s(z)$ is described with an exponential function containing an a parameter (see Šimůnek and Suarez, 1993) which was set to 0.0015 m^{-1} in our simulations.

In SOILCO$_2$, there is no time dependency of microbial respiration (i.e., γ_s is not linked to RMI), and the Verhulst–Pearl logistic growth function is used to describe root growth from differences in vertical root penetration depth. The use of these assumptions revealed a poor fit to our data set. For our simulations, R_{init} and r were fixed at 2 g DW and 2.4×10^{-6} g s^{-1}, respectively. Assuming linear root growth, the r was calculated by dividing the measured root biomass at the end of a similar mesocosm experiment (13.7 g at 70 days after sowing and 64.5 days after plant emergence; Thaysen et al., 2014b) with 64.5 days of plant growth. The R_{init} was then calculated from multiplication of the r with the number

of days after plant emergence at simulation time zero (i.e., 15 days after sowing minus 5.5 days of plant emergence). The γ_{p0} and γ_{s0} parameters were set to 0.8 µmol m^{-2} s^{-1} g^{-1}_{DWroot}, assuming equal contributions of microbial and root respiration to the total R_s (mean of reported contributions of root respiration to the total R_s of 10–90 %; Swinnen, 1994; Hanson et al., 2000; Kocyigit and Rice, 2006; Moyano et al., 2007). When multiplied by the root mass at the end of the experiment, the sum of γ_{p0} and γ_{s0} resulted in a CO_2 production of 16 µmol m^{-2} s^{-1}, which was within the calculated range of the actual average CO_2 production of 15–31 µmol m^{-2} s^{-1} in planted mesocosms (Sect. 3.4). An overview of all applied parameters is given in Table S1 in the Supplement.

The simulated CO_2 efflux from the ecosystem to the atmosphere is essentially the soil respiration, R_s, because there is no plant module in this conceptual model. Hence, our ER measurements could not be directly compared to the simulated CO_2 efflux. Anticipating that (1) canopy respiration was roughly 50 % of the total plant respiration (Poorter et al., 1990; Loveys et al., 2002), and (2) root respiration accounted for 50 % of the total R_s (see above), we corrected the ER by a factor of 0.67 to get an estimate of the R_s.

2.3.3 Root solute uptake

Root solute uptake was simulated based on literature values on the average plant content of major ions. Average plant nutrient contents were (µmol g DW plant^{-1}; from Marschner, 1995): K^+, 250; Ca^{2+}, 125; Mg^{2+}, 80; PO_4^{3-}, 60; SO_4^{2-}, 30; Na^+, 0; total N (modeled as NO_3^-), 1000. The daily influx per g DW root, J, was calculated by multiplying the average plant nutrient content by the rate of total plant biomass increase over the experiment (1.05 g d^{-1}) and dividing by the total root mass at the end of the experiment ($\sim$ 13.7 g). The root mass dependent influx, J_{TIME} (mol s^{-1}), was then obtained by multiplication of J with the RMI and the normalized vertical root distribution, $f_p(z)$, (Eq. 7).

$$J_{TIME} = J \cdot RMI \cdot f_{p(z)}. \quad (7)$$

Because the root length was fixed at 30 cm (Sect. 2.3.1), but the root mass within this depth increased by the RMI, root solute uptake was simulated to increase linearly over time within the A horizon.

Root cation uptake was described by simultaneous excretion of protons, except for K^+ for which Na^+ was assumed to be excreted. Anion uptake was modeled by OH^- excretion. This approach for root solute uptake modeling is in agreement with general knowledge on root nutrient uptake mechanisms (Marschner, 1995).

2.3.4 Geochemistry

Aqueous speciation and complexation were accounted for using PHREEQC (Parkhurst and Appelo, 2013) and the wateq4f.dat database. Cation exchange capacities and initial compositions were as measured from soil extractions (Kjøller et al., 2004). Initial exchanger compositions were equilibrated with a solution composition in contact with a pCO_2 of 1 % and with 0.3 meq L^{-1} alkalinity, as measured on day 15 after sowing. Charge balance of the initial solution was achieved using Li^+ and an equilibrium constant for the exchange reaction of log $k = -100$. Nutrient irrigation was modeled using the Hoagland solution composition diluted 1 : 1 by H_2O.

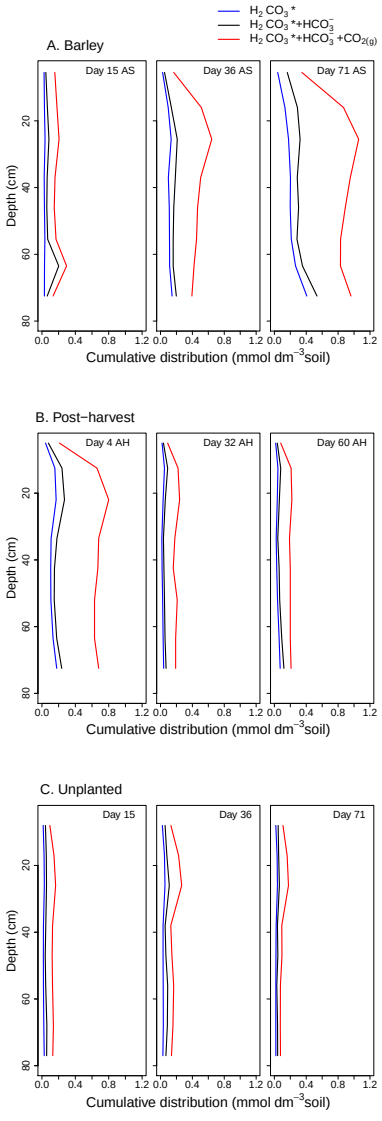

Figure 2. Distribution of inorganic carbon between dissolved inorganic carbon (DIC) species and $CO_{2(g)}$ at the start (day 15 in **(a)** and **(c)**, day 4 in **(b)**), in the middle (day 36 in **(a)** and **(c)**, day 32 in **(b)**) and at the end (day 71 in **(a)** and **(c)**, day 60 in **(b)**), of experiments in mesocosms with barley **(a)**, post-harvest **(b)** and in unplanted mesocosms **(c)**. Shown are the means for each treatment. AS represents after sowing, AH represents after harvest. The concentration of carbonate was negligible compared to the other species and is not shown.

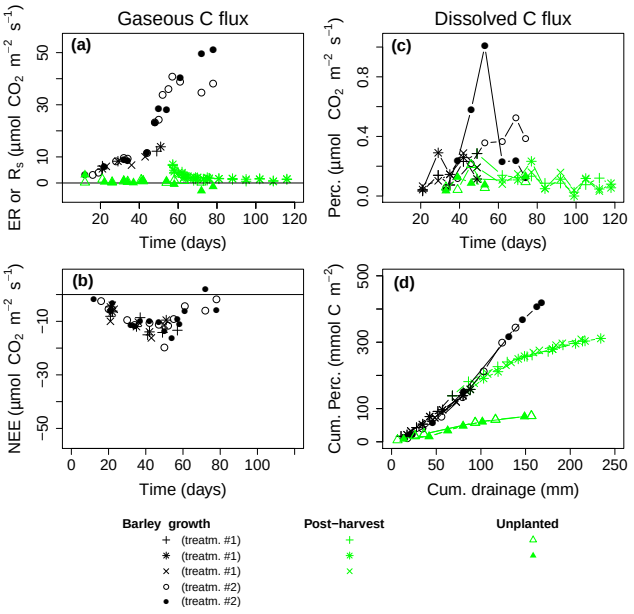

Figure 3. Gaseous and dissolved CO_2 fluxes from mesocosms. **(a)**: ecosystem respiration (ER) from barley mesocosms during growth (black) and soil respiration (R_s) from barley mesocosms after harvest and unplanted mesocosms (green). **(b)**: net ecosystem exchange (NEE) from mesocosms with barley. **(c)**: dissolved inorganic carbon (DIC) percolation flux recalculated into gaseous efflux unit. **(d)**: cumulative DIC percolation flux as a function cumulative drainage.

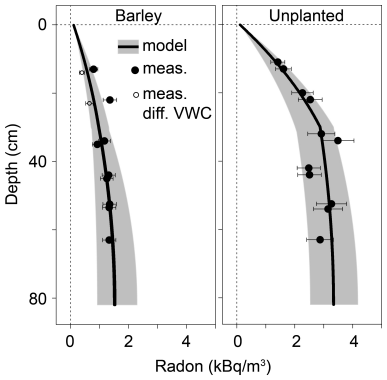

Figure 4. Measured and modeled Rn profiles in barley mesocosms of growth treatment #2 and in unplanted mesocosms. Open symbols indicate Rn measurements taken at lower volumetric water content (VWC) than the remaining samples. Grey shaded areas designate model calculations carried out with diffusivities within the stated confidence intervals (see text).

3 Results

3.1 Distribution of total inorganic carbon between gas and aqueous phase species

The total inorganic C distributed between gaseous and aqueous phase species (i.e., $CO_{2(g)}$ and DIC) increased during barley growth and decreased after harvest (Fig. 2a and b). Over time, inorganic C was mainly found as $CO_{2(g)}$ and changed little beyond 20 cm depth. A downward moving front of elevated [DIC] was not visible. The latter was expected in the middle to bottom range of the C horizon due to the downward movement of initially present pore water. In unplanted mesocosms, the amount of inorganic C and distribution between species hardly changed over the course of the experiment (Fig. 2c).

3.2 CO_2 exchange and aboveground biomass

The ER increased with time during plant growth (Fig. 3a). After harvest of the aboveground biomass, the R_s declined logarithmically (Fig. 3a). The R_s from unplanted mesocosms was much lower than from barley mesocosms and was relatively constant. The negative NEE, i.e., ecosystem CO_2 uptake, increased with plant age up to day 54 after which it decreased to less negative values similar to those observed 20 days after sowing (Fig. 3b). Soil surface temperatures were 20–23 °C during measurements (Fig. S1). The aboveground biomass in mesocosms of the barley growth treatment #2 was $2918 \pm 83\,\mathrm{g\,m^{-2}}$.

3.3 DIC percolation

The DIC percolation flux varied considerably in all treatments but tended to increase with plant growth (range: 0.02–1 µmol $CO_2\,m^{-2}\,s^{-1}$), decrease after harvest (0.03–0.3 µmol $CO_2\,m^{-2}\,s^{-1}$), and remain fairly constant in unplanted soil (0.01–0.2 µmol $CO_2\,m^{-2}\,s^{-1}$; Fig. 3c).

The cumulative amount of DIC that leached from barley mesocosms in the first growth treatment and post-harvest was 303–311 mmol C m^{-2} at a cumulative drainage of 212–234 mm (Fig. 3d). This drainage corresponded to an estimated 1.8–2.0 times the initially water-filled pore volumes, with 0.6–0.7 times the water-filled pore volumes flushed during growth. The average [DIC] during the pre-harvest and post-harvest periods was 1.8–2.0 and 1.1–1.3 mmol L^{-1}, respectively.

In the second barley growth treatment, the cumulative amount of DIC leached was 360–440 mmol C m^{-2} and significantly higher than the 80–82 mmol C m^{-2} leached from the corresponding unplanted mesocosms (Fig. 3d). The cumulative drainage from barley mesocosms of the second barley treatment and from unplanted mesocosms was 139–168 and 141–158 mm, respectively (Fig. 3d) and corresponded to 1.3–1.5 and 1.1–1.3 times the initially water-filled pore volumes. The average [DIC] in mesocosms of the second barley treatment and in unplanted mesocosms was 2.5 and 0.4–0.5 mmol L^{-1}, respectively. The cumulative DIC percolation fluxes from all mesocosms were highly correlated with the cumulative drainages (Fig. 3d; $R^2 = 0.96$–0.99).

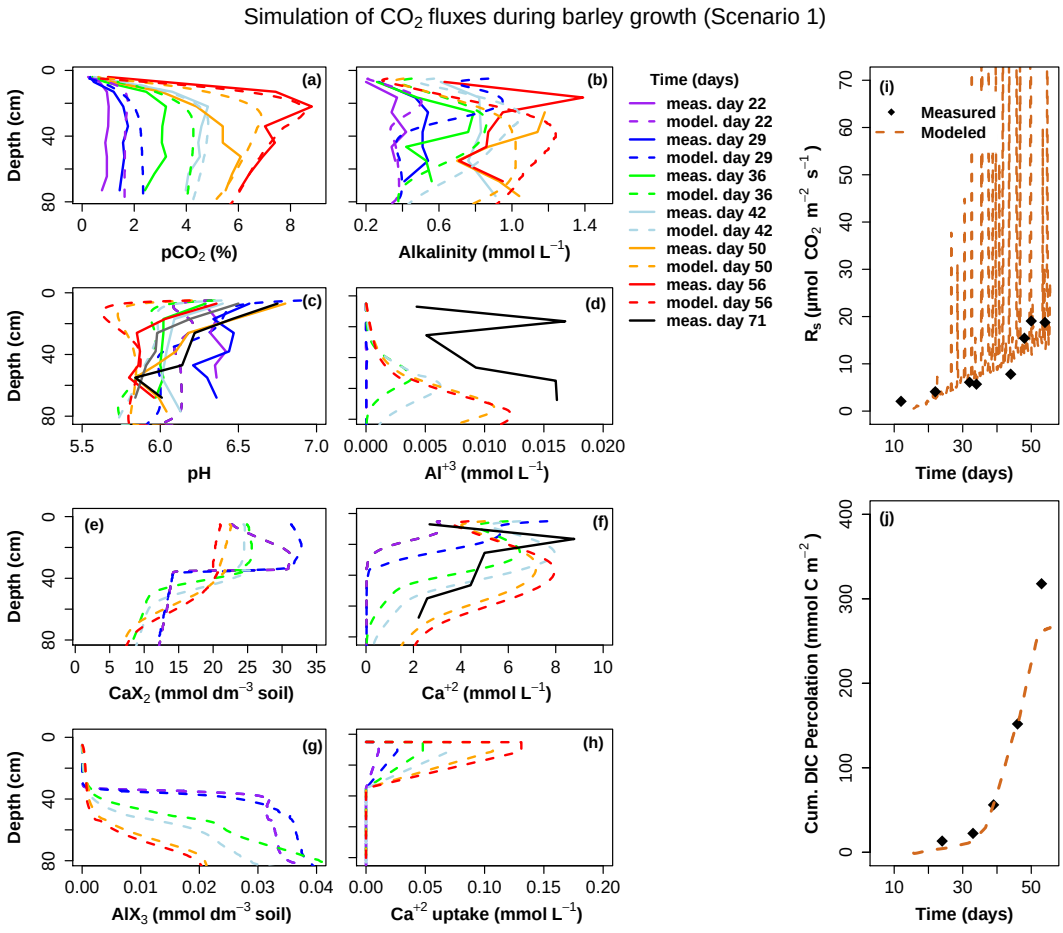

Figure 5. Measured (full lines or dots) and simulated (dashed lines) temporal variation (expressed in days after sowing) of soil air pCO_2 **(a)**, alkalinity **(b)**, pH **(c)**, Al^{3+} **(d)**, CaX_2 **(e)**, Ca^{2+} **(f)**, AlX_3 **(g)**, Ca^{2+} root uptake **(h)**, R_s **(i)** and cumulative DIC percolation **(j)** during barley growth. Geochemical reactions in simulations were described by root nutrient uptake and cation exchange (scenario 1). In **(i)** small fluctuations in the simulated R_s around the baseline arise from diurnal temperature variations. Large fluctuations are numerical noise caused by the fact that the numerical solution does not fully obey the von Neumann stability criteria.

3.4 CO_2 emission partitioning

The cumulative CO_2 effluxes to the atmosphere from unplanted and planted soil (barley growth #2) during 78 days of experiment, using linear interpolation between measurements, were 0.4–1.1 and 32.8–33.4 mol C m^{-2}, respectively (not shown). The corresponding cumulative DIC percolation fluxes of 0.080–0.082 and 0.36–0.44 mol C m^{-2}, respectively, constituted 7.3–20.5 and 1.6–2.0 % of the aboveground CO_2 emission. The cumulative post-harvest CO_2 efflux to the atmosphere during 60 days of experiment was 2.4–2.7 mol C m^{-2} at a cumulative DIC percolation flux of 0.15–0.16 mol C m^{-2}, corresponding to a relative magnitude of the cumulative DIC percolation flux compared to the cumulative aboveground CO_2 efflux of 5.6–6.7 %.

3.5 Soil diffusivity and CO_2 production

The Rn emanation rates of the soil A and C horizons were 4.93 ± 0.46 and 2.65 ± 0.13 atoms s^{-1} kg^{-1}, respectively. At a VWC of ~ 20 % in the A horizon, the Rn concentration [Rn] was 1.5 times larger in unplanted mesocosms than in planted mesocosms, with a difference of ~ 1000 Bq m^{-3} (Fig. 4). The bulk soil diffusivity was determined by comparing measured [Rn] profiles at a given VWC with modeled [Rn] at different bulk diffusivities. The code RnMod3d could reproduce the Rn profiles in unplanted mesocosms using bulk diffusivities of 0.6×10^{-6} and 2.0×10^{-6} m^2 s^{-1} for the A and C horizon, respectively. For barley mesocosms, the bulk diffusivities for the A and C horizon were 2.1×10^{-6} and 1.9×10^{-6} m^2 s^{-1}, respectively (Fig. 4). The confidence intervals in Fig. 4 mark the range of diffusivities at which agreement between measured and modeled [Rn] could be achieved. Modeled soil bulk diffusivities of the unplanted

A and C horizons showed reasonable agreement with bulk diffusivities of 0.44×10^{-6} and 0.9×10^{-6} m^2 s^{-1}, respectively, calculated from empirical formulas in Rogers and Nielson (1991) and Andersen (2001) (see Text S1 in the Supplement).

The CO_2 diffusion coefficient in unplanted and barley mesocosms was estimated to $1.2–2.3 \times 10^{-6}$ and $1.8–6.8 \times 10^{-6}$ m^2 s^{-1}, respectively, using the Rn bulk diffusivities (Eq. 1). Average soil CO_2 production as calculated from the range for the A horizon bulk diffusivities was 1.0–1.8 and 15.1–31.1 µmol m^{-2} s^{-1} for mesocosms of the unplanted and barley growth #2 treatment, respectively, where CO_2 production during barley growth increased from ∼ 5 to 59 µmol m^{-2} s^{-1} (confidence intervals: 3.5–7.4 to 30–87 µmol m^{-2} s^{-1}).

3.6 Modeling of CO_2 fluxes

The CO_2 diffusivity and production estimates (Sect. 3.5) were used to simulate the measured CO_2 fluxes in one mesocosm of the second barley growth treatment. Different geochemical constraints were applied in three scenarios. In scenario 1, root nutrient uptake was coupled to cation exchange. Scenario 2 had cation exchange and equilibrium (saturation index = 0) for amorphous aluminium hydroxide, $Al(OH)_{3(a)}$, as the soil solution chemistry in the mesocosms revealed a possible control by $Al(OH)_{3(a)}$ (Fig. S2 in the Supplement). Scenario 3 was equal to scenario 2 except that root nutrient uptake was included. The fit of scenarios 2 and 3 to measured parameters was poor (not shown) and hence the discussion of our modeling is limited to scenario 1.

Due to the dependency of the pCO_2 and the R_s on the VWC, a correct description of the VWC in the mesocosms at any given point in time was crucial. The dependency of the DIC percolation flux on the drainage flux implied a need for an exact simulation of the drainage flux. Both water flow and drainage flux were generally well described (Fig. S5 in the Supplement).

The temporal variation of the simulated pCO_2 and R_s captured the main trends in the observations (Fig. 5a, i). However, in the upper part of the mesocosm, the simulated pCO_2 was somewhat higher than the measured pCO_2 up to day 36 despite a good agreement between simulated and observed topsoil VWC (Fig. S5) and the R_s (Fig. 5i). The simulated cumulative DIC percolation provided a good fit to the measured data up to day 46 but underestimated the measured DIC percolation on day 53 (Fig. 5j) due to lower simulated alkalinity towards the mesocosm bottom (Fig. 5b).

A general increase in alkalinity over time was caused by the high root uptake of NO_3^- that exceeded uptake of any other plant nutrients (Fig. S3 in the Supplement) and caused a net excretion of OH^-. This counteracted the pH drop caused by CO_2 dissolution and buffered the pH around 5.6–6.0 (Fig. 5c). Mismatch between the simulated and the calculated pH were largely caused by differences between measured and simulated alkalinity and pCO_2. The simulated high near-surface pH (Fig. 5c) was due to low pCO_2 caused by the diffusional loss of CO_2 and high alkalinity caused by evaporation processes (see tracer simulation, Fig. S4 in the Supplement).

Scenario 1 simulated increasing $[Al^{3+}]$ and $[Ca^{2+}]$ with time that approached the measurement on day 71 (Fig. 5d and f, respectively). Increasing $[Al^{3+}]$ resulted from displacement of exchanger-bound Al by cations in the incoming nutrient solution. High $[Al^{3+}]$ led to supersaturation of $Al(OH)_{3(a)}$ (not shown), in accordance with Fig. S3 in the Supplement. Calcium was displaced on the A horizon exchanger as well (Fig. 5e), resulting in increasing $[Ca^{2+}]$ with time. However, the largest increase in $[Ca^{2+}]$ resulted from irrigation with nutrient solution and subsequent upconcentration due to evapotranspiration (Fig. 5f). Root uptake rates of Ca^{2+} (and other nutrients) were small compared to $[Ca^{2+}]$ in the soil solution (Figs. 5h, S3) but the accompanying release/uptake of protons had a big impact on the soil alkalinity and pH (Fig. 5b and c). Exchanger-bound Al and Ca were displaced by K (not shown), probably due to higher $[K^+]$ in the nutrient solution compared to other ions, and the high ionic strength of the nutrient solution (13.9 mmol kg^{-1} water) (Appelo and Postma, 2005).

4 Discussion

In this work, we have quantified the inorganic C dynamics in planted and unplanted soil mesocosms representing the vadose zone of a cultivated podzol. The data were generated from a detailed collection of gaseous and aqueous samples and from subsequent modeling enabled by the novel implementation of SOILCO$_2$ into HP1. We show that inorganic C dynamics in ecosystems are not well described from measurements of the CO_2 pools and fluxes alone, and that biogeochemistry has a potentially major impact on the movement of dissolved CO_2 in the vadose zone. In the following section, our results are discussed in the context of soil type effects on CO_2 fluxes and differences between mesocosm and field studies are addressed.

4.1 Soil respiration: gaseous CO_2 efflux

The R_s and the pCO_2 (Figs. 3a and S1) in unplanted mesocosms were generally in agreement with field studies on a range of different arable soils (Table 2). In barley mesocosms, the ER and the pCO_2 were generally higher than in published field studies but were in accordance with pot-grown barley in humic clay (Simojoki et al., 1991) (Table 3).

Higher respiration rates in barley mesocosms than in the field were probably a function of a larger plant biomass, as also observed by Simojoki et al. (1991). The aboveground and root biomass was 3–4 times and 2–5 times higher, respectively, than the values reported from field studies

Table 2. Ranges of soil respiration (R_s) and soil partial pressure of CO_2 (pCO_2) in unplanted mesocosms as compared to other studies (one in pots, four in the field). NA represents not available, VWC represents volumetric water content.

R_s ($\mu mol\,m^{-2}\,s^{-1}$)	pCO_2 (%)	Crop	Soil type	Soil texture	Soil surface temperature (°C)	Daytime air temperature (°C)	VWC (%)	Reference
−3.0–3.2	0.2–1.2	Fallow	Podzol	Coarse sand	22–23	18	20–25	This study (mesocosms)
∼ 0.7–1.5	NA	Fallow	Gleyic Cambisol	Sandy soil	18–22	NA	NA	(Weihermüller et al., 2009) (pot experiment)
∼ 0.05–3.7	NA	Fallow	Arenosol	Sandy soil	3–20	−10–28	10–25	(Herbst et al., 2008)
NA	0.5 ± 0.1	Fallow	Fine Montmorillonitic, Mesic Udollic Ochraqualfs	Silt loam	15–20	13–15	27–30	(Buyanovsky and Wagner, 1983)
1.5–8	NA	Fallow	Orthic Humic Gleysol	Loam	10–26	NA	25–40	(Rochette et al., 1992)
−2–10	NA	Fallow	Endocalcari–Epihypogleyic Cambisol	Clay loam	19–27	11–22	NA	(Feizene et al., 2008)

Table 3. Ranges of ecosystem respiration (ER) and soil partial pressure of CO_2 (pCO_2) during growth in barley mesocosms as compared to other studies (two in mesocosms, seven in the field). NA represents not available, VWC represents volumetric water content.

ER ($\mu mol\,m^{-2}\,s^{-1}$)	pCO_2 (%)	Crop	Soil type	Soil texture	Soil surface temperature (°C)	Daytime air temperature (°C)	VWC (%)	Reference
0.8–52	0.2–8.8	Barley	Podzol	Coarse sand	20–24	18	20–25	This study (mesocosms)
NA	∼ 2–10	Barley	Humic clay soil	Clay	NA	NA	15–32	(Simojoki et al., 1991) (mesocosms)
NA	2–6	Barley	Podzol	Coarse sand	−7 to 29 (mean ∼ 8)	8 (mean)	6–34	Our field site
∼ 1–16	NA	Barley	Eutric Cambisol	Sandy soil with high humus content	12–23	18–30	13–23	(Lohila et al., 2003)
NA	0.3–2	Barley	Eutric Cambisol	Coarse sandy loam over gravely sand	NA	∼ 9.3 (mean)	∼ 17–33	(Walmsley et al., 2011)
0.2–16	NA	Barley	Haplic Phaeozem	Silty clay loam	−2 to 22	NA	21–27	(Moyano et al., 2007)
−3–9	NA	Barley, winter wheat	Endocalcari-Epihypogleyic Cambisol	Clay loam	19–26	11–22	NA	(Feizene et al., 2008)
2.8–4.5	0.3–6	Winter wheat	Montmorillonitic, Mesic Udollic Ochraqualfs	Fine silt loam	10–25	13–27	15–30	(Buyanovsky and Wagner, 1983)
2.3-07.5	NA	Barley	Orthic Humic Gleysol	Loam	10–19	NA	10–35	(Rochette et al., 1992)

(Barraclough and Leigh, 1984; Xu and Juma, 1992; Malhi and Gill, 2002; Lohila et al., 2003; Walmsley et al., 2011). Additional increase in the ER may have been caused by 3 to 5 °C higher day- and night time temperatures in the growth room than in the field (e.g., Kotroczo et al., 2008). Some artificial increase in the ER (and a decrease in the NEE) can be expected to result from the application of the chamber for CO_2 exchange measurements since the plant canopy covered a larger surface area than the surface area of the mesocosms (Fig. 1a).

The soil CO_2 efflux to the atmosphere was about 1 order of magnitude higher in planted mesocosms than in unplanted mesocosms at peak time (Fig. 3a). As previously shown by Lee (1997) this revealed a strong impact of vegetation on CO_2 dynamics in the unsaturated zone. Post-harvest R_s were higher than from unplanted soil, indicating a stimulation of microbial respiration by root-derived substrates (Kuzyakov, 2002). Respiration rates after harvest were within the range of previously reported R_s from sandy soil ($0.5\,\mu mol\,C\,m^{-2}\,s^{-1}$) (Heitkamp et al., 2012) and silty clay loam ($1–11\,\mu mol\,C\,m^{-2}\,s^{-1}$) (Moyano et al., 2007). The relatively high post-harvest R_s and its rapid decline are in accordance with the high root biomass in mesocosms combined with a fast depletion of labile C from sandy soil (Heitkamp et al., 2012).

4.2 Percolation: DIC fluxes

The DIC percolation flux was calculated from the alkalinity, the pCO_2 at the mesocosm bottom and the drainage flux but was primarily a function of the latter two variables. The smaller effect of the alkalinity on the downward DIC flux was caused by the low soil pH that shifted DIC primarily towards $H_2CO_3^*$ (Fig. 2). The absence of a downward moving DIC front was caused by the fact that $H_2CO_3^*$ is a direct function of the pCO_2 that was constant with depth (Fig. S1).

The higher pCO_2 in barley mesocosms caused about a 4 times higher DIC percolation flux than in unplanted mesocosms at similar drainage (Fig. 3c and d). Average post-harvest [DIC] were significantly higher than the average [DIC] in the percolation water from unplanted soil but may have partly been influenced by high [DIC] during plant growth due to incomplete exchange of the initial water-filled pore volume of during barley growth in the first barley treatment. The latter implies that high [DIC] arising from high pCO_2 conditions at the mesocosm top during barley growth were not transported all the way to the mesocosm outlet.

The DIC percolation flux and the average [DIC] under barley were within the range of reported values for cropland soil (Table 4). Further comparison of the [DIC] in the percolation water is impeded by the numerous factors influencing soil pCO_2 and the [DIC] (see Sects. 1 and 4.1). The DIC

Table 4. Dissolved inorganic carbon (DIC) percolation fluxes from different types of cropland.

Crop	Annual DIC Percolation ($g\,C\,m^{-2}\,yr^{-1}$)	Drainage ($mm\,yr^{-1}$)	Average DIC ($mmol\,L^{-1}$)	Soil type	Soil texture	Carbonates in soil	Country	Reference
Soybean/winter wheat	7.6–8.0	782	0.8–0.9 (dissolved CO_2 only)	Fluvisol	Clay loam over loam	No	Japan	(Minamikawa et al., 2010)
Onion	13.2	1200	0.9	Mesic Mollic Fluvaquent	Aquic clay	No	Japan	(Sawamoto et al., 2003)
Cropland, not further specified	~ 1.9–10.2 (estimated from figure)	241–537	~ 0.7–1.6 (estimated from figure)	Fluvioglacial sands and gravel	Sandy loam over gravelly sand	Not specified	Ireland	(Jahangir et al., 2012)
Cropland, not further specified	19.4	975	1.7	Stagnol	Silt loam	No	Germany	(Kindler et al., 2011)
Maize	9.2–18	~ 250–400 (estimated from figure)	3–3.8	Mesic Typic Argiudoll	Fine silt loam	Not specified	USA	(Brye et al., 2002)
Winter wheat/ winter barley	2.0	88	1.9	Luvisol	Sandy loam	Yes	Germany	(Siemens et al., 2012)
Spring barley	20.1	603	2.8	Eutric Cambisol	Coarse sandy loam over gravely sand	Sporadic bands in subsoil	Ireland	(Walmsley et al., 2011)
Barley	4.3–5.3*	139–168	2.5	Podzol	Coarse sand	Artificially added to the A horizon	Denmark	This study
Cropland, not further specified	13.3	189	5.9	Calcaric Cambisol	Silt loam	Yes	France	(Kindler et al., 2011)

* DIC percolation fluxes in during barley growth (treatment #1) for a growth period of 78 days.

percolation flux from unplanted soil was similar to the previously reported percolation fluxes from sandy forest soils (Kindler et al., 2011).

4.3 CO_2 emission partitioning and controls on CO_2 fluxes in the vadose zone

Our measurements revealed a pivotal influence of vegetation on CO_2 fluxes in the vadose zone as both upward and downward transport of CO_2 was strongly increased in planted mesocosms (Fig. 3). The cumulative DIC percolation flux was small relative to the cumulative aboveground CO_2 efflux. Results from planted mesocosms (1.6–2.0 %) were higher than the global emission flux partitioning (0.26 %) (Raich and Potter, 1995; Kessler and Harvey, 2001) but lower than a 2.5 % fraction reported for an onion field (Sawamoto et al., 2003). The relatively higher ratio between cumulative DIC percolation flux and the cumulative R_s in unplanted mesocosms resulted from lower cumulative R_s in unplanted soil that was further decreased by periods of net uptake of CO_2 (Fig. 3a). The potential for manipulating the emission balance by increasing the DIC export to the groundwater via irrigation is substantial after harvest where the absence of plant transpiration facilitates fast percolation of water through the soil and where relatively high soil pCO_2 may transmit to increases in the [DIC].

The interpretation of CO_2 fluxes in mesocosms needs to take into account the high plant biomass density in mesocosms, the constant summer conditions in the climate chamber and the coarse-sanded, acidic soil of this study. Elevated biomass of plants grown at relatively high temperature increased the soil respiration which again increased both upward and downward flux of CO_2. Smaller [Rn] in barley mesocosms (Fig. 4) indicated that root growth and decay increased the soil diffusivity (by $\sim 1.5 \times 10^{-6}\,m^{-2}\,s^{-1}$). This may have enhanced the R_s, implying a decreased net uptake of atmospheric CO_2 (NEE) by the plant-soil ecosystem. Increased diffusivity due to the presence of biopores and cracks has indeed been reported (Holford et al., 1993; Hoff, 1997). However, some reduction in the [Rn] in planted soil may have been caused by Rn removal via plant transpiration (Lewis and MacDonell, 1990; Jayaratne et al., 2011). In any case, the high soil diffusivity of the coarse sand and the relatively low soil pH of ~ 6 caused much less downward transport of DIC compared to the CO_2 emission to the atmosphere (Fig. 3).

Modeling of the CO_2 fluxes using different explanatory scenarios was a valuable tool for identifying the key processes behind the observed evolution in the dissolved CO_2 fluxes. Scenario 1 (root nutrient uptake coupled to cation exchange) was in accordance with previous demonstrations of slight soil alkalinization when nitrate is the dominating inorganic N species (Marschner et al., 1991; Weligama et al., 2010). However, our modeling of the nutrient uptake remains somewhat uncertain due to lack of data for actual nutrient uptake. A control of $Al(OH)_{3(a)}$ on the soil solution was unlikely but other buffering processes such as the dissolution of small pieces of lime (Fig. S2) may be possible.

Soil pCO_2 and R_s were hardly affected by any buffering process, despite the low subsoil pH that caused partitioning of DIC towards $H_2CO_3^*$ and some degassing to $CO_{2(g)}$ (Fig. 2). This is in accordance with existing knowledge that mineral reactions affecting the carbonate system have only marginal effects on the pCO_2 (Kuzyakov, 2006).

The modified SOILCO$_2$ model made use of several simplifications of reality, one of them being the linkage of the y_s to the RMI without inclusion of a bulk soil y_s. However, due to the dense root growth in the A horizon (see Thaysen et al., 2014b, Fig. 1 and Sect. 4.1) plant root independent y_s was probably negligible in the A horizon. The exponential decline in the y_s with soil depth by the $f_s(z)$ (Eqs. 3–5) further implied that the y_s in the C horizon was small compared to the topsoil. Hence, for the experimental conditions of this study, the omission of a plant-root independent y_s in our model seems justified.

5 Conclusions

The DIC percolation flux of ~ 5 mmol C m^{-2} d^{-1} during barley growth was ~ 1.6–2.0 % of the R_s at increased plant biomass and elevated soil pCO_2 compared to the field situation. After harvest, the magnitude of the DIC percolation flux was lowered to ~ 2.5 mmol C m^{-2} d^{-1} but the importance of DIC percolation flux for the overall cropland CO_2 emission increased to ~ 6–7 % of the R_s.

At constant conditions of temperature and water content, the R_s was controlled by the production and diffusivity of CO_2 in the soil, both of which were increased by plant growth. The DIC percolation flux was primarily controlled by the recharge flux and the pCO_2 due to the low soil pH in the acidic soil of our study. Modeling suggested that nutrient buffering during root nitrate uptake dominated any mineral control on the soil solution in planted mesocosms.

This study showed that the integration of experimental and modeling work is a powerful tool in advancing process-understanding of CO_2 fluxes in the vadose zone. Our findings are important for improving current base understanding of CO_2 partitioning in the vadose zone and may be included in the optimization of climate models. Further research is needed to outline the effect of different crops and soil amendments on the CO_2 emission portioning of croplands.

The Supplement related to this article is available online at doi:10.5194/bg-11-7179-2014-supplement.

Acknowledgements. The authors thank Mette Hem Flodgaard, Anja C. Nielsen, Christina Lynge and Szymon Kopalski for skilled technical and laboratory support during sampling procedures and analysis, as well as Nina Wiese Thomsen for invaluable assistance in sampling events, and Rasmus Jakobsen and Jirka Šimůnek for support and discussion during the modeling. The project was financed by the Danish Council for Strategic Research (DSF-09-067234).

Edited by: P. Stoy

References

Ambus, P., Petersen, S. O., and Soussana, J. F.: Short-term carbon and nitrogen cycling in urine patches assessed by combined carbon-13 and nitrogen-15 labelling, Agr. Ecosyst. Environ., 121, 84–92, doi:10.1016/j.agee.2006.12.007, 2007.

Andersen, C.: Numerical modelling of radon-222 entry into houses: An outline of techniques and results, Sci. Total Environ., 272, 33–42, 2001.

Archer, D. and Brovkin, V.: The millennial atmospheric lifetime of anthropogenic CO_2, Climatic Change, 90, 283–297, 2008.

Appelo, C. A. J. and Postma, D.: Geochemistry, groundwater and pollution, 2, 649 pp., Balkema, 2005.

Barker, T., Bashmakov, I., Bernstein, L., Bogner, J. E., Bosch, P. R., Dave, R., Davidson, O. R., Fisher, B. S., Gupta, S., Halsnæs, K., Heij, G. J., Kahn Ribeiro, S., Kobayashi, S., Levine, M. D., Martino, D. L., Masera, O., Metz, B., Meyer, L. A., Nabuurs, A., Najam, G.-J., Nakicenovic, N., Rogner, H.-H., Roy, J., Sathaye, J., Schock, R., Shukla, P., H. Sims, R. E., Smith, P., Tirpak, D. A., Urge-Vorsatz, D., and Zhou, D.: Technical summary, Cambridge University Press, Cambridge, UK, and New York, USA, 25–93, 2007.

Barnes, R. T. and Raymond, P. A.: The contribution of agricultural and urban activities to inorganic carbon fluxes within temperate watersheds, Chem. Geol., 266, 318–327, 2009.

Barraclough, P. B. and Leigh, R. A.: The growth and activity of winter wheat roots in the field: The effect of sowing date and soil type on root growth of high-yielding crops, J. Agr. Sci., 103, 59–74, 1984.

Brye, K. R., Gower, S. T., Norman, J. M., and Bundy, L. G.: Carbon budgets for a prairie and agrosystems: Effects of land use and interannual variability, Ecol. Appl., 12, 962–979, 2002.

Buyanovsky, G. A. and Wagner, G. H.: Annual cycles of carbon dioxide level in soil air, Soil Sci. Soc. Am. J., 47, 1139–1145, 1983.

Chung, S.-O. and Horton, R.: Soil heat and water flow with a partial surface mulch, Water Resour. Res., 23, 2175–2186, 1987.

Feizene, D., Povilaitis, V., and Kadziene, G.: Springtime soil surface respiration and soil vapour flux in different long-term agroecosystems, Liet. Moksl. Akad. (Spausd.), 54, 216–225, 2008.

Fierer, N., Chadwick, O. A., and Trumbore, S.: Production of CO_2 in soil profiles of a California annual grassland, Ecosystems, 8, 412–429, 2005.

Hanson, P. J., Edwards, N. T., Garten, C. T., and Andrews, J. A.: Separating root and soil microbial contributions to soil respiration: A review of methods and observations, Biogeochemistry, 48, 115–146, 2000.

Heitkamp, F., Jäger, N., Flessa, H., Raupp, J., and Ludwig, B.: Effect of fertilization on respiration from different sources in a sandy soil of an agricultural long-term experiment, Arch. Agron. Soil Sci., 58, 933–944, 2012.

Hendry, M. J., Mendoza, C. A., Kirkland, R., and Lawrence, J. R.: An assessment of a mesocosm approach to the study of microbial respiration in a sandy unsaturated zone, Ground Water, 39, 391–400, 2001.

Herbst, M., Hellebrand, H. J., Bauer, J., Huisman, J. A., Šimůnek, J., Weihermüller, L., Graf, A., Vanderborght, J., and Vereecken, H.: Multiyear heterotrophix soil respiration: Evaluation of a coupled CO_2 transport and carbon turnover model, Ecol. Model., 214, 271–283, 2008.

Hoagland, D. R. and Amon, D. I.: The water-culture method for growing plants without soil, College of Agriculture, University of California, Berkeley, 347, 32 pp., 1950.

Hoff, A.: Radon transport in fractured soil: Laboratory experiments and modelling, Risø-R-975(EN), Risø National Laboratory, Roskilde, Denmark, 151 pp., 1997.

Hoffmann, G. J. and van Genuchten, M. T.: Soil properties and efficient water use: Water management for salinity control, limitations and efficient water use in crop production, edited by: Taylor, H. M., Jordan, W. R., and Sinclair, T. R., American Society of Agronomy, Madison, WI, USA, 73–85, 1983.

Holford, D. J., Schery, S., Wilson, J. L., and Phillips, F. M.: Modeling radon transport in dry, cracked soil, J. Geophys. Res., 98, 567–580, 1993.

Houghton, R. A.: Balancing the global carbon budget, Annu. Rev. Earth Pl. Sc., 35, 313–347, doi:10.1146/annurev.earth.35.031306.140057, 2007.

Huxman, T. E., Cable, J. M., Ignace, D. D., Eilts J. A., English, N. B., Weltzin, J., Williams, D. G.: Response of net ecosystem gas exchange to a simulated precipitation pulse in a semi-arid grassland: The role of native versus non-native grasses and soil texture, Oecologia, 141, 295–305, 2004.

IPCC: Summary for policymakers, in: Climate Change, 2007: The physical science basis, Contribution of working group I to the fourth assessment report of the Intergovernmental Panel on Climate Change, edited by: Solomon, S., Qin, D., Manning, M., Chen, Z., Marquis, M., Averyt, K. B., Tignor, M., and Miller, H. L., IPCC, Cambrigde, UK, and New York, NY, USA, 2007.

Jacques, D., Šimůnek, J., Mallants, D., and van Genuchten, M. T.: Modeling coupled hydrologic and chemical processes: Long-term uranium transport following phosphorus fertilization, Vadose Zone J., 7, 698–711, 2008.

Jahangir, M. M. R., Johnston, P., Khalil, M. I., Hennessey, D., Humpreys, J., Fenton, O., and Richards, K. G.: Groundwater: A pathway for terrestrial C and N losses and indirect greenhouse gas emissions, Agric. Ecosyst. Environ., 159, 40–48, 2012.

Jassal, R., Black, A., Novak, M., Morgenstern, K., Nesic, Z., and Gaumont-Guay, D.: Relationship between soil CO_2 concentrations and forest-floor CO_2 effluxes, Agr. Forest Meteorol., 130, 176–192, doi:10.1016/j.agrformet.2005.03.005, 2005.

Jayaratne, E. R., Ling, X., and Morawska, L.: Role of vegetation in enhancing radon concentration and ion production in the atmosphere, Environ. Sci. Technol., 45, 6350–6355, 2011.

Kessler, T. J. and Harvey, C. F.: The global flux of carbon dioxide into groundwater, Geophys. Res. Lett., 28, 279–282, 2001.

Kindler, R., Siemens, J., Kaiser, K., Walmsley, D. C., Bernhofer, C., Buchmann, N., Cellier, P., Eugster, W., Gleixner, G., Grünwalds, T., Heim, A., Ibrom, A., Jones, S., Jones, M., Lehuger, S., Loubet, B., McKenzie, R., Moors, E., Osborne, B., Pilegaard, K., Rebmann, C., Saunders, M., Schmidt, M. W. I., Schrumpf, M., Seyferth, J., Skiba, U., Soussana, J.-F., Sutton, M. A., Tefs, C., Vowinckel, B., Zeeman, M. J., and Kaupenjohann, M.: Dissolved carbon leaching from soil is a crucial component of the net ecosystem carbon balance, Glob. Change Biol., 17, 1167–1185, doi:10.1111/j.1365-2486.2010.02282.x, 2011.

Kjøller, C., Postma, D., and Larsen, F.: Groundwater acidification and the mobilization of trace metals in a sandy aquifer, Environ. Sci. Technol., 38, 2829–2835, 2004.

Kocyigit, R. and Rice, C. W.: Partitioning CO_2 respiration among soil, rhizosphere microorganisms, and roots of wheat under greenhouse conditions, Commun. Soil Sci. Plan., 37, 1173–1184, doi:10.1080/00103620600623392, 2006.

Kotroczo, Z., Fekete, I., Toth, J. A., Tothmeresz, B., and Balazsy, S.: Effect of leaf- and rootlitter manipulation for carbon-dioxide efflux in forest soil, Cereal Res. Commun., 36, 663–666, 2008.

Kuzyakov, Y.: Review: Factors affecting rhizosphere priming effects, J. Plant Nutr. Soil Sc., 165, 382–396, 2002.

Kuzyakov, Y.: Sources of CO_2 efflux from soil and review of partitioning methods, Soil Biol. Biochem., 38, 425–448, doi:10.1016/j.soilbio.2005.08.020, 2006.

Lal, R.: Soil carbon sequestration, FAO, SOLAW background thematic report-TR04B, 2011.

Lee, M.-S., Nakane, K., Nakatsubo, T., Mo, W.-H., and Koizumi, H.: Effects of rainfall events on soil CO_2 flux in a cool temperate deciduous broad-leaved forest, Ecol. Res., 17, 401–409, 2002.

Lee, R. W.: Effects of carbon dioxide variations in the unsaturated zone on water chemistry in a glacial-outwash aquifer, Appl. Geochem., 12, 347–366, 1997.

Lewis, B. G. and MacDonell, M. M.: Release of radon-222 by vascular plants: Effect of transpiration and leaf area, J. Environ. Qual., 19, 93–97, 1990.

Lohila, A., Aurela, M., Regina, K., and Laurila, T.: Soil and total ecosystem respiration in agricultural fields: Effect of soil and crop type, Plant. Soil., 251, 303–317, doi:10.1023/A:1023004205844, 2003.

Loveys, B. R., Scheurwater, I., Pons, T. L., Fitter, A. H., and Atkin, O. K.: Growth temperature influences the underlying components of relative growth rate: An investigation using inherently fast- and slowgrowing plant species, Plant. Cell Environ., 25, 975–987, 2002.

Maier, M., Schack-Kirchner, H., Hildebrand, E. E., and Schindler, D.: Soil CO_2 efflux vs. soil respiration: Implications for flux models, Agr. Forest. Meteorol., 151, 1723–1730, doi:10.1016/j.agrformet.2011.07.006, 2011.

Malhi, S. S. and Gill, K. S.: Fertilizer N and P effects on root mass of bromegrass, alfalfa and barley, J. Sustain. Agr., 19, 51–63, 2002.

Marschner, H.: Mineral nutrition of higher plants, Second Edition ed., Academic Press Limited, London, 861 pp., 1995.

Marschner, H., Haussling, M., and George, E.: Ammonium and nitrate uptake rates and rhizosphere pH in nonmycorrhizal roots of norway spruce [Picea-abies (L) Karst], Trees-Struct. Func., 5, 14–21, 1991.

Millington, R. J. and Quirk, J. M.: Permeability of porous solids, T. Faraday Soc., 57, 1200–1207, 1961.

Minamikawa, K., Nishimura, S., Sawamoto, T., Nakajima, Y., and Kazuyuki, Y.: Annual emissions of dissolved CO_2, CH_4, and N_2O in the subsurface drainage from three cropping systems, Glob. Change Biol., 16, 796–809, 2010.

Moyano, F. E., Kutsch, W. L., and Schulze, E. D.: Response of mycorrhizal, rhizosphere and soil basal respiration to temperature and photosynthesis in a barley field, Soil Biol. Biochem., 39, 843–853, 2007.

Mualem, Y.: Hydraulic conductivity of unsaturated porous media: Generalized macroscopic approach, Water Resour. Res., 14, 325–334, 1978.

Parkhurst, D. and Appelo, C. A. J.: Description of input and examples for PHREEQC version 3 – A computer program for speciation, batch-reaction, one-dimensional transport, and inverse geochemical calculations: U.S. Geological Survey, Techniques and Methods, book 6, chap. A43, 497 pp., available at: http://pubs.usgs.gov/tm/06/a43, 2013.

Poorter, H., Remkes, C., and Lambers, H.: Carbon and nitrogen economy of 24 wild species differing in relative growth rate, Plant Physiol., 94, 621–627, 1990.

Raich, J. W. and Potter, C. S.: Global patterns of carbon-dioxide emissions from soils, Global Biogeochem. Cy., 9, 23–36, 1995.

Richards, L. A.: Capillary conduction of liquids through porous mediums, Physics, 1, 318–333, 1931.

Robertson, P., Paul, E. A., and Harwood, R. R.: Greenhouse gases in intensive agriculture: Contributions of individual gases to the radiative forcing of the atmosphere, Science, 289, 1922–1925, 2000.

Rochette, P., Desjardins, R. L., Gregorich, E. G., Pattey, E., and Lessard, R.: Soil respiration in barley (*Hordeum vulgare*) and fallow fields, Can. J. Soil Sci., 72, 591–603, 1992.

Rogers, V. C. and Nielson, K. K.: Correlations for predicting air permeabilities and ^{222}Rn diffusion coefficients in soils, Health Phys., 61, 225–230, 1991.

Sawamoto, T., Kusa, K., Hu, R., and Hatano, R.: Dissolved N_2O, CH_4, and CO_2 emissions from subsurface-drainage in a structured clay soil cultivated with onion in central Hokkaido, Japan. Soil Sci. Plant Nutr., 49, 31–38, 2003.

Schimel, D. S.: Terrestrial ecosystems and the carbon cycle, Glob. Change Biol., 1, 77–91, 1995.

Schlesinger, W. H.: Carbon balance in terrestrial detritus, Annu. Rev. Ecol. Syst., 8, 51–81, 1973.

Siemens, J., Pacholski, A., Heiduk, K., Giesemann, A., Schulte, U., Dechow, R., Kaupenjohann, M., and Weigel, H.-J.: Elevated air carbon dioxide concentrations increase dissolved carbon leaching from a cropland soil, Biogeochemistry, 108, 135–148, 2012.

Simojoki, A., Jaakkola, A., and Alakukku, L.: Effect of compaction on soil air in a pot experiment and in the field, Soil Till. Res., 1991, 75–186, 1991.

Šimůnek, J. and Suarez, D. L.: Modeling of carbon-dioxide transport and production in soil 1, Model development, Water Resour. Res., 29, 487–497, 1993.

Šimůnek, J., Jacques, D., van Genuchten, M. T., and Mallants, D.: Multicomponents geochemical transport modeling using Hydrus-1-D and HP1, J. Am. Water Resour. As., 42, 1537–1547, 2006.

Šimůnek, J., Sejna, M., Saito, H., Sakai, M., and van Genuchten, M.: The Hydrus-1-D software package for simulating the movement of water, heat, and multiple solutes in variably saturated media, Version 4.16, HYDRUS Software Series 3, Department of Environmental Sciences, University of California Riverside, Riverside, California, USA, 240 pp., 2013.

Steefel, C. I., DePaolo, D. J., and Lichtner, P. C.: Reactive transport modeling: An essential tool and a new research approach for the earth sciences, Earth Planet. Sc. Lett., 240, 539–558, doi:10.1016/j.epsl.2005.09.017, 2005.

Solomon, S., Qin, D., Manning, M., Alley, R. B., Berntsen, T., Bindoff, N. L., Chen, Z., Chidthaisong, A., Gregory, J. M., Hegerl, G. C., Heimann, M., Hewitson, B., Hoskins, B. J., Joos, F., Jouzel, J., Kattsov, V., Lohmann, U., Matsuno, T., Molina, M., Nicholls, N., Overpeck, J., Raga, G., Ramaswamy, V., Ren, J., Rusticucci, M., Somerville, R., Stocker, T. F., Whetton, P., Wood, R. A., and Wratt, D.: Technical Summary, in: Climate Change 2007: The physical science basis. Contribution of working group I to the fourth assessment report of the Intergovernmental Panel on Climate Change, IPCC, Cambridge, United Kingdom and New York, NY, USA, 92 pp., 2007.

Suarez, D. L. and Šimůnek, J.: Modeling of carbon-dioxide transport and production in soil 2, Parameter selection, sensitivity analysis, and comparison of model predictions to field data, Water Resour. Res., 29, 499–513, 1993.

Swinnen, J.: Rhizodeposition and turnover of root-derived organic material in barley and wheat under conventional and integrated management, Agric. Ecosyst. Environ., 51, 115–128, 1994.

Thaysen, E. M., Jessen, S., Ambus, P., Beier, C., Postma, D., and Jakobsen, I.: Technical Note: Mesocosm approach to quantify dissolved inorganic carbon percolation fluxes, 11, 1077–1084, 2014a.

Thaysen, E. M., Jessen, S., Postma, D., Jakobsen, R., Jacques, D., Ambus, P., Laloy, E., and Jakobsen, I.: Effects of lime and concrete waste on vadose zone carbon cycling, Vadose Zone J., 13, 1–11, doi:10.2136/vzj2014.07.0083, 2014b.

Trumbore, S.: Carbon respired by terrestrial ecosystems - recent progress and challenges, Glob. Change Biol., 12, 141–153, doi:10.1111/j.1365-2486.2006.01067.x, 2006.

van Genuchten, M.: A closed-form equation for predicting the hydraulic conductivity of unsaturated soils, Soil Sci. Soc. Am. J., 44, 892-]898, 1980.

van Genuchten, M. T.: A numerical model for water and solute movement in and below the root zone, U.S. Salinity laboratory, USDA, Riverside, CA, USA, 1987.

Vermeulen, S. J., Campbell, B. M., and Ingram, S. I.: Climate change and food systems, Annu. Rev. Env. Resour., 37, 195–222, 2012.

Vrugt, J. A., Robinson, B. A., and Hyman, J. M.: Self-adaptive multimethod search for global optimization in real-parameter spaces, IEEE T. Evolut. Comput., 13, 243–259, 2009.

Walmsley, D. C., Siemens, J., Kindler, R., Kirwan, L., Kaiser, K., Saunders, M., Kaupenjohann, M., and Osborne, B. A.: Dissolved carbon leaching from an Irish cropland soil is increased by reduced tillage and cover cropping, Agr. Ecosyst. Environ., 142, 393–402, doi:10.1016/j.agee.2011.06.011, 2011.

Weihermüller, L., Huisman, J. A., Graf, A., Herbst, M., and Sequaris, J.-M.: Multistep outflow experiments to determine soil physical and carbon dioxide production parameters, Vadose Zone J., 8, 772–782, 2009.

Weligama, C., Sale, P. W. G., Conyers, M. K., Liu, D. L., and Tang, C.: Nitrate leaching stimulates subsurface root growth of wheat and increases rhizosphere alkalisation in a highly acidic soil, Plant Soil., 328, 119–132, 2010.

Xu, J. G. and Juma, N. G.: Above- and below-ground net primary production of four barley (*Hordeum vulgare L.*) cultivars in western Canada, Can. J. Plant Sci., 72, 1131–1140, 1992.

Zhang, J. Y., Lin, Z. B., Zhang, R. D., and Shen, J.: Effects of simulated rainfall events on soil carbon transformation, Aust. J. Soil Res., 48, 404–412, doi:10.1071/Sr09182, 2010.

Zhu, B. and Cheng, W.: Rhizosphere priming effect increases the temperature sensitivity of soil organic matter decomposition, Glob. Change Biol., 17, 2172–2183, 2011.